---

**Article:**
Andrews, J., Button, D. and Reaney, I.M. orcid.org/0000-0003-3893-6544 (2020) Advances in cold sintering : Improving energy consumption and unlocking new potential in component manufacturing. Johnson Matthey Technology Review, 64 (2). pp. 219-232. ISSN 2056-5135

https://doi.org/10.1595/205651320x15814150061554

---

https://doi.org/10.1595/205651320X15814150061554 *Johnson Matthey Technol. Rev.*, 2020, **64**, (2), 219–232

JOHNSON MATTHEY
TECHNOLOGY REVIEW
www.technology.matthey.com

# Advances in Cold Sintering

## Improving energy consumption and unlocking new potential in component manufacturing

**Jessica Andrews*, Daniel Button and Ian M. Reaney**
Functional Materials and Devices Group, Department of Materials Science and Engineering, The University of Sheffield, Western Bank, Sheffield, S10 2TN, UK

***Email:** jandrews2@sheffield.ac.uk

Ceramics are traditionally sintered at high temperatures (~80% melting temperature ($T_m$)). There are numerous incentives to reduce processing temperature: the reduction in processing energy; integration of polymeric and non-noble metals; greater control of microstructure and final component geometries. 'Cold sintering' has been developed as a novel method of densification which uses a transient liquid phase, pressure and heat to achieve dense ceramics. This review explores the process of cold sintering and its potential to densify various ceramic materials and components at low temperatures (<300°C), primarily describing recent results at The University of Sheffield, UK.

## 1. Introduction

Sintering is a crucial stage in the manufacturing of dense ceramic products from a green body. Archaeologists have dated some of the earliest ceramic artefacts to 24,000 BCE (1) and sintering was empirically developed over thousands of years prior to the appearance of modern sintering theories (1). Traditionally, sintering to create dense products requires heat treatment up to 80% of $T_m$ to promote the transport of material to eliminate pores. Such high temperatures are costly in terms of energy and can be restrictive in the manufacture of functional ceramic devices which often require integration of metals and polymers that suffer from volatility, melting, interaction and mismatch in thermal expansion with the ceramic. This leads to complications in the production of components, which include warping, delamination and the high cost of inert noble metals such as platinum and palladium. **Figure 1** shows the compatibility of several materials at various sintering temperatures.

Reducing sintering temperatures is a critical strategy in the goal of decarbonising foundation industries. A number of methods have been proposed to reduce sintering temperature, or more precisely the energy for densification, these include the addition of sintering aids, the utilisation of Joule heating through processes such as spark plasma sintering (SPS) and flash sintering and most recently cold sintering (2). There have also been some investigations into combinations of cold sintering and SPS-flash sintering.

Sintering aids are often utilised to reduce conventional sintering temperatures and typically form a liquid phase flux through which mass is more rapidly transported than within the solid state. In electroceramics, lithium-doping of barium titanate has been shown to successfully reduce sintering temperatures: Kimura *et al*. demonstrated a reduction from 1300°C to 1000°C (3) and Randall *et al*. to 750°C by the addition of 15 mol% lithium fluoride (4). Many other sintering aids have been investigated, but none have been found to reduce $BaTiO_3$ sintering temperatures to <900°C (2, 5), which is desirable for metal internal electrode technologies in multilayer devices (6).

Flash sintering is a field assisted sintering technique (FAST) for the consolidation of ceramics. A green body is placed in contact with electrodes in a furnace, an electric field is applied and the furnace heated until a specific temperature or field and the 'flash' phenomenon occurs (7). The densification occurs rapidly and significantly reduces the sintering temperature, for example Downs *et al*.

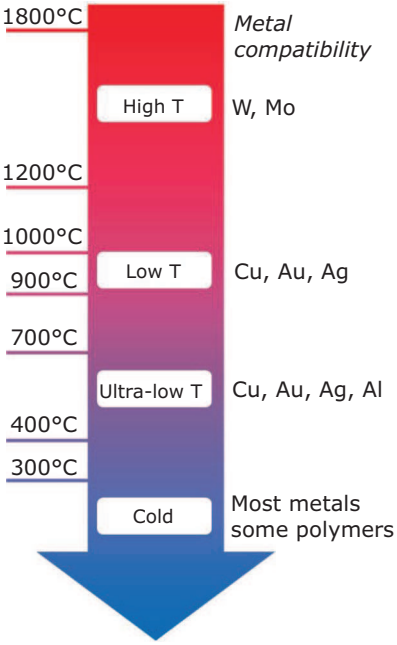


Fig. 1. Material compatibility with ceramic sintering temperatures

densified cubic yttria-stabilised zirconia (8YSZ) at 390–1000°C below conventional temperatures (8). There are a number of challenges to be overcome in flash sintering including the formation of hot spots in larger components due to the electric current concentration (7).

SPS is a field assisted, high pressure method which is particularly useful for materials that are difficult to fabricate using conventional technology such as bismuth telluride-based thermoelectrics (9). It typically utilises a graphite die filled with powder which is subjected to high pressure and temperature in the presence of a field. Not only is the temperature to achieve densification reduced but also the sintering time (<1 min). Oxides however, require re-oxidation post densification as the graphite die reduces the compound, which to some extent negates the benefits of SPS.

Cool SPS exploits high pressure in a vacuum to densify materials with low decomposition temperatures or unfavourable phase transitions at <400°C (10, 11). Compounds such as manganese(II) sulfate (96%), potassium bis-(carbonato)cuprate(II) (94–95%), sodium bis-(carbonato)cuprate(II) (97–98%), ammonium iron(III) diphosphate (95–98%) and zirconia (66–80%) have been densified *via* this method at 300–600 MPa and 300–400°C.

The highly energy intensive nature of conventional ceramic sintering contributes heavily to the cost of the materials and products and to the environmental impact of manufacturing. The energy required to sinter $BaTiO_3$ conventionally is 2800 kJ $g^{-1}$. A comparison of energy consumption for several sintering methods is shown in **Table I**. Compared with conventional sintering, an energy reduction of ~99% has been reported for $BaTiO_3$ cold sintered at 300°C (2), thereby demonstrating its potential importance to foundation industries such as ceramics which are required to decarbonise.

**Table I Comparison of Energy Consumption for Barium Titanate of Sintering Techniques (2)**

| Sintering method | Energy consumption, kJ $g^{-1}$ |
|---|---|
| **Solid state** | 2800 |
| **Liquid phase** | 2000 |
| **Field assisted** | 1050 |
| **Microwave** | 540 |
| **Fast firing** | 130 |
| **Cold sintering** | 30 |

## 2. Cold Sintering

Cold sintering or the cold sintering process (CSP) is a novel method of sintering ceramics first introduced by Jantunen and coworkers (12) but developed further at Pennsylvania State University, USA, by Randall and colleagues. CSP utilises a liquid phase to aid rearrangement and interdiffusion of the particles alongside pressure and modest heat to dramatically reduce the sintering temperature (**Figure 2**). The proposed mechanisms of CSP densification are closely related to those in liquid phase sintering (2). During cold sintering, powdered material is mixed with a transient liquid in which it is partially soluble. The moistened powder is then placed into a die and pressure (100–500 MPa) and heat (<300°C) are applied to aid rearrangement of the particles and the reprecipitation of the solid material (13). The development of the process has mainly been on a material by material basis, optimising parameters empirically.

Prior to research emerging from Randall *et al*. at Pennsylvania State University, Yamasaki *et al*. described a combined process of hydrothermal reactions with isostatic pressing referred to as hydrothermal hot pressing (HHP) to densify ceramics at <200°C in 1986 (14). The process was used to demonstrate the densification of a

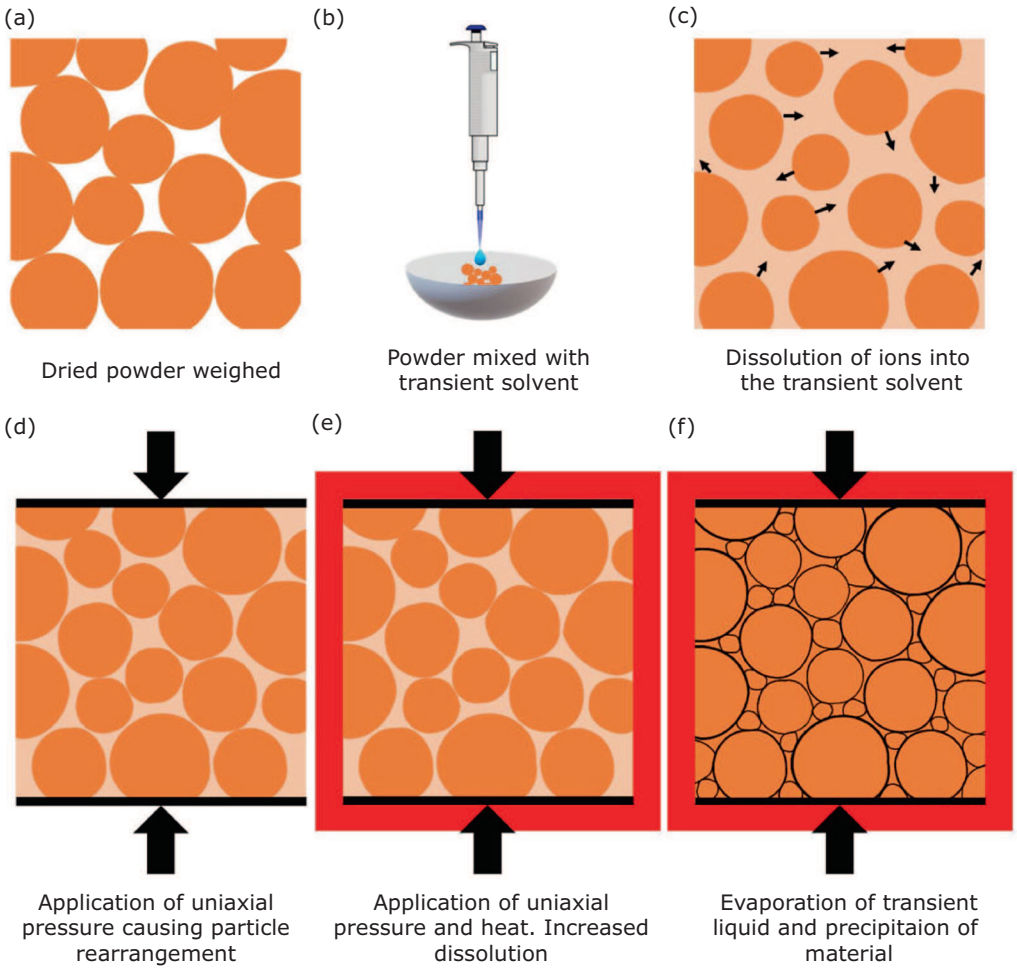


Fig. 2. Schematic illustrating the different stages of the cold sintering process

range of materials including silicates, cements, $BaTiO_3$, porous anatase and hydroxyapatite ceramics (14–16). The process was applied to bonding hydroxyapatite with metal and densifying ceramics which decompose at low temperatures. Cold sintering has many similarities with HHP such as the requirement for a liquid phase to facilitate mass transport and the occurrence of dissolution and precipitation reactions. HHP was inspired by natural geographical phenomenon and is now considered to be a subset of the broader definition of CSP and the equipment for HHP (17).

## 2.1 Congruently Dissolving Materials

### 2.1.1 Molybdates

Lithium molybdate (LMO) is a hygroscopic material which is congruently soluble in water and was one of the first materials used to demonstrate cold sintering (4, 13, 18). LMO is conventionally sintered at 540°C but *via* cold sintering it can be densified at 120°C with the addition of 2–10 wt% distilled water under applied pressure (12, 17, 18). The properties of cold sintered LMO are comparable with conventional samples but a slight increase in dielectric loss is thought to relate to residual hydroxyl groups at the grain boundaries (12).

Materials related to LMO such as sodium molybdate (NMO) can also be densified *via* cold sintering. Whilst NMO is not hygroscopic, it is highly soluble in water making it another ideal candidate for cold sintering. NMO is conventionally sintered at 610°C, whilst the material can be cold sintered at 150°C with the addition of 5–10 wt% water and the application of 200 MPa of pressure. Wang *et al*. achieved relative densities of 87% after conventional sintering but 96% after cold sintering. The dielectric properties of NMO are also comparable between conventional and cold sintered. An increase in permittivity ($\varepsilon_r$) is observed (conventional: 11.6, CSP: 12.7), due to increased

 

density whilst residual hydroxyl groups increased dielectric loss (19, 20).

As LMO and NMO are readily densified *via* cold sintering, they have been used as a starting point to create many composites with other materials with more favourable properties, but which are harder to cold sinter such as barium hexaferrite, sodium bismuth molybdate and bismuth lithium vanadium molybdate (19, 21, 22).

### 2.1.2 Zinc Oxide

Zinc oxide has also gained interest as a material that can be densified *via* cold sintering. ZnO is wide band-gap (3.4 eV) semiconductor traditionally used in electronics such as varistors and requires temperatures in excess of 1100°C to sinter (23, 24). The high temperatures for conventional sintering leads to grain coarsening and other effects deleterious to the electrical properties and therefore methods of reducing sintering temperature have been widely investigated. Several studies have successfully cold sintered ZnO at ≤300°C. Unlike molybdate compounds, ZnO has limited solubility in water and therefore an alternative transient solvent such as aqueous acetic acid or zinc acetate (Zn-Ac) is utilised to achieve sufficient dissolution to promote densification (25, 26).

Recent work at The University of Sheffield has investigated the effects of pressure and temperature on the cold sintering of ZnO. Samples of ZnO were produced at temperatures 125–300°C and pressures of 187–375 MPa with 25–30 wt% of 1 M acetic acid. Scanning electron microscopy (SEM) of cold sintered ZnO showed that temperature and pressure have a significant effect on grain growth and morphology, helping to corroborate previous work by Funahashi *et al.* and Kang *et al*. (25, 26).

Funahashi studied cold sintering of ZnO using a wide variety of pressures, temperatures and concentrations of acetic acid (0.1–17.5 M) and water for comparison. The presence of the acetic acid was critical to achieve high density, with 1.0 M the optimal concentration. Pressures of 387 MPa combined with 300°C were reported to produce the highest densities from the test pressures and temperatures. The lower pressure of 77 MPa did produce high densities however no neck-growth was observed (26), in agreement with work done in The University of Sheffield. Pellets pressed at 250 MPa at 300°C showed high density (>98% theoretical) and grain growth but no necking, **Figure 3(c)**. When pressure was increased to 374 MPa necking is observed (**Figure 3(d)**)

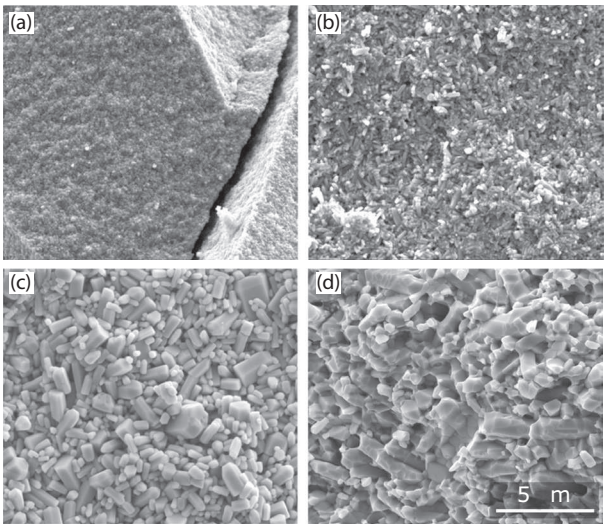


Fig. 3. Fracture surface SEM micrographs of cold sintered ZnO fabricated at The University of Sheffield at a range of temperatures and pressures: (a) 120°C and 250 MPa; (b) 200°C and 250 MPa; (c) 300°C and 250 MPa; (d) 300°C and 375 MPa. All micrographs are at same magnification

producing a sample with a microstructure similar to conventional sintering.

Kang *et al*. studied a large range of processing conditions, including the use of various solvent chemicals and the effect of pressure, temperature, pH and ion concentration. Initial findings agreed with Funahashi with pressure promoting necking and temperature having the largest effect on grain growth (25, 26). However, it was proposed that pressure has a threshold below which densities are significantly affected. Beyond this threshold, densification becomes pressure independent. Other chemicals explored by Kang *et al*. (other than acetic acid or Zn-Ac) include hydrochloric acid, sulfuric acid, zinc chloride and zinc sulfate but only 70–75% densities were achieved, as well as unwanted cement and hydroxide phases (25). Densification was independent of pH due mainly to the presence of $Zn^{2+}$ and acetate ions. The exchange of $Zn^{2+}$ ions through solution enabled by applied pressure is the largest contributor to densification (25). Secondary phases observed by Kang *et al*. were also present, contradicting earlier suggestions that samples were single phase (26). Raman analysis showed evidence of residual acetate or Zn-Ac (25) which was confirmed in our studies. **Figure 4** shows a comparison of ZnO cold sintered at 125°C and 300°C compared to a conventionally sintered sample produced at The University of Sheffield. At 125°C and 300°C, three

 

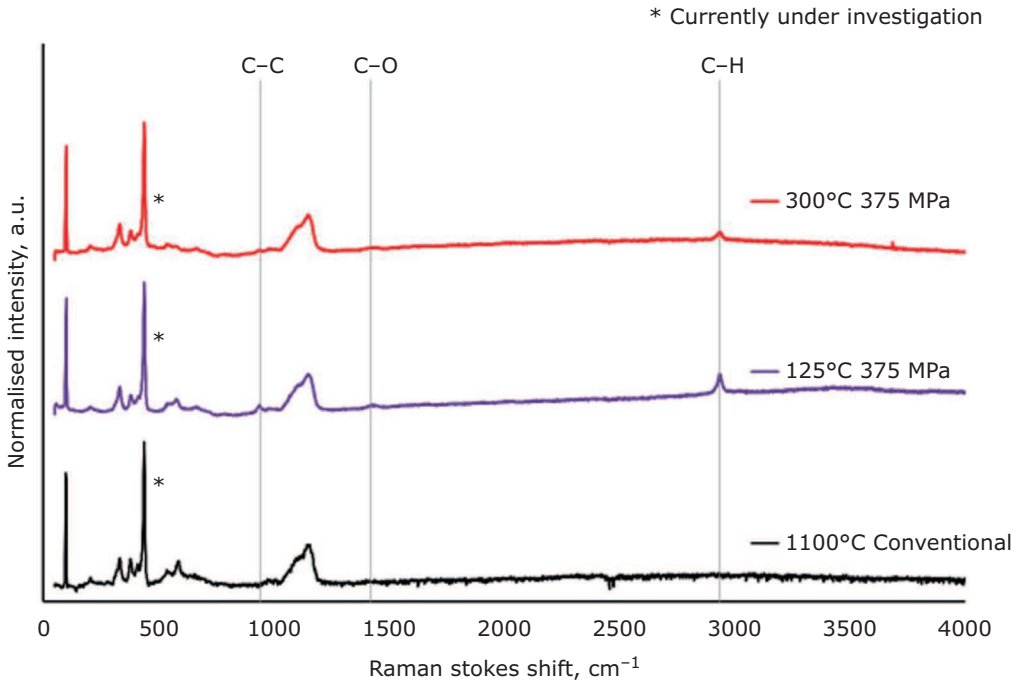


Fig. 4. Raman spectra of ZnO comparing sintering conditions. Conventional sintering at 1100°C for 2 h, cold sintering performed at 125°C, 375 MPa and 300°C, 375 MPa with 30 wt% 1 M acetic acid

peaks are observed which are not present in the conventional sample. The peak at ~943 cm$^{-1}$ is typical of a C–C bond, ~1435 cm$^{-1}$ a C–O bond and finally at ~2930 cm$^{-1}$ a mode characteristic of a C–H and the peak ~650 cm$^{-1}$ is still under investigation. These organic peaks are weaker in the 300°C sample, suggesting that some of the acetate has been removed. Acetate decomposes at ~225°C consistent with this hypothesis.

Gonzalez-Julian *et al*. densified ZnO *via* cold sintering and a combined cold sinter-FAST/SPS method, using Kelvin probe force microscopy (KPFM) on resulting samples, to better understand the mechanisms behind cold sintering (27). For both CSP and CSP-SPS, powders were moistened with 1.6–3.2 wt% distilled water or a 0.5% Zn–Ac solution. Samples were then sintered according to parameters in **Table II**. The addition of Zn–Ac to the transient solvent was found to significantly reduce the onset temperature of densification from 90–130°C to ~25°C at all pressures. This demonstrates the crucial role of powder dissolution in densification *via* cold sintering.

KPFM was used to analyse the surface potentials of samples sintered *via* CSP-SPS at 150 MPa. The addition of water increased surface potential compared to the as-received powder, which implies an increase in defect concentration. A contrasting effect is seen with the addition of Ac-$H_2O$, where surface potentials are reduced indicating a lower defect concentration, which the authors attribute to the observed grain growth. The increase in surface potential indicates that the solvent phase not only promotes transport but also raises the sintering potential through the creation of activation energy lowering defects, as $OH^-$ and $H^+$ ions diffuse into the surface of the crystal structure (25–27).

From impedance spectroscopy, ZnO densified using Ac-$H_2O$ had the highest conductivity with significantly lower total activation energy than other conditions. The bulk activation energy of ZnO was found to be significantly reduced by sintering with both water and acetate, whereas

**Table II Parameters Used by Gonzalez-Julian *et al.* (27) to Create CSP and CSP-SPS Samples**

| | CSP | CSP-SPS |
|---|---|---|
| **Solvent content, wt%** | 1.6–3.2 $H_2O$<br>3.2 $H_2O$ + 0.5 Zn-Ac | 1.6 $H_2O$<br>1.6 $H_2O$ + 0.5 Zn-Ac |
| **Temperature ramp rate, °C min$^{-1}$** | 20 | 100 |
| **Holding temperature, °C** | 250 | 250 |
| **Pressure, MPa** | 150, 300 | 100, 125, 150 |

the grain boundary ($E_a$) was found to be increased with $H_2O$ and decreased with Ac-$H_2O$. This lowering of activation energy is thought to be due to the manufacture of highly defective diffusion pathways, which helps to encourage sintering at low temperatures.

Overall Gonzalez-Julian *et al*. theorised the liquid phase has five main roles during the CSP in ZnO: (a) a better initial packing of the powder material due to interparticle friction; (b) dissolution of $Zn^{2+}$ and $O^{2-}$ ions from the powder surface; (c) formation of defects in ZnO crystals due to $H^+$ and $OH^-$ diffusion; (d) formations of highly defective diffusion pathways between grains and (e) elimination of carbonates. These effects are thought to be further enhanced by the presence of the acetate phase by improving dissolution. This paper indicates that the liquid phase has a more complex role than first suggested by initial studies; better understanding of defect chemistry effects is in understanding and improving the results achieved from the CSP.

To unite cold and flash sintering, Nie *et al*. studied the effect of an aqueous transient liquid phase on flash sintered ZnO. An electrode green body produced by uniaxial pressing was placed in a flash chamber and flowing wet argon + 5% hydrogen was introduced after 1 h. The conductivity of the hydrated pellet increased by a factor of four compared to the unhydrated form ($3 \times 10^{-7}$ S cm$^{-1}$ to ~$7 \times 10^{-3}$ S cm$^{-1}$). The presence of water was found to trigger flash sintering at room temperature due to the higher conductivity, producing relative densities of ~98%. The water was also proposed to assist with densification *via* mass transport due to partial dissolution of the substrate (28).

## 2.2 Non-Congruently Dissolving Materials

As already discussed, Li, NMO and ZnO are relatively easy to cold sinter and coarse powders can be densified with the addition of water or acetic acid as the transient solvent. To cold sinter a wider variety of materials, with a broader range of properties, several methods are employed, such as reducing the particle size to nanoscale, thereby increasing the reactivity of the powder and altering liquid additive to include more complex acids, alkalis or ionic solvents.

In cases where the powder dissolves incongruently, a method of hydrothermal assisted cold sintering is utilised through reactive intermediate phases. The liquid utilised in cold sintering of incongruent materials is often a solution containing a deep eutectic reaction precursor to form the desired products at temperatures below that of a solid-state process (29–32).

When particles of $BaTiO_3$ are exposed to water, Ba ions leach from the surface, leaving a titanium-rich layer (33). To cold sinter $BaTiO_3$, Guo *et al*. utilised nanoscale particles of $BaTiO_3$ and a barium hydroxide on titania suspension in deionised water. This prevents the dissolution of Ba during cold sintering and the $Ba(OH)_2$ and $TiO_2$ react to form $BaTiO_3$ during annealing at 700–900°C.

Strontium titanate is conventionally sintered at over 1400°C (34). Boston *et al*. developed a method of cold sintering for $SrTiO_3$ which utilised reactive intermediate phases (29). Nanoscale $SrTiO_3$ and $TiO_2$ powders were mixed with 0.2 ml of a 1.5 M strontium chloride aqueous solution with 1.5 M equivalent of anatase nanoparticles. The mixture was pestle and mortared to produce a free-flowing powder which was then pressed at 750 MPa for 10 min at room temperature before increasing to 180°C for 60 min. After cold sintering, a 4 h heat treatment at 950°C was utilised to promote microreactions between $SrCl_2$ and $TiO_2$ intermediate phases, forming $SrTiO_3$. Electrical testing of cold sintered $SrTiO_3$ showed similar trends to conventionally sintered materials, however the relative permittivity values exhibited frequency dependence. Particle size in the conventionally sintered samples is shown to affect the permittivity and loss (**Table III**).

## 2.3 Challenges for Cold Sintering

Cold sintering is an exciting area for development in ceramic science. There are however a number of challenges which will need to be overcome to

**Table III Relative Permittivity and Tan δ from 25–250°C for Cold *vs*. Conventional Sintered $SrTiO_3$ (29)**

| | Nanoscale | | Micron-scale | |
|---|---|---|---|---|
| | Permittivity | Tan δ | Permittivity | Tan δ |
| **Conventional** | 130–210 | 0–0.55 | 120–180 | 0–0.14 |
| **Cold** | 70–120 | 0–0.21 | 70–120 | 0–0.21 |

improve the commercial prospects of this new technology.

### 2.3.1 Processing Parameters

Most developments in cold sintering so far have been on an empirical, material-specific, 'trial and error' basis. A greater understanding of the mechanisms and how they relate to processing parameters will allow a wider range of materials to be densified *via* cold sintering. There are numerous processing parameters which can be altered to tailor the densification of material during cold sintering, including composition of transient liquid phase, volume of transient liquid required, pressure, temperature and powder particle size.

The transient phase should allow for the congruent dissolution of the solid phase or react to form a desirable composition upon heating during sintering or subsequent heat treatment. Therefore, it is important to understand the dissolution behaviour of the ceramic within the temperature range of sintering. The amount of liquid used during cold sintering is mostly quoted in weight percent of the solid phase. This does not consider the effect of surface area, far greater for nano- as opposed to micropowders. The purpose of pressure during cold sintering is the rearrangement of particles, but it also plays a more complex role in dissolution, grain growth and activation of reactions due to inhomogeneous pressure distributions.

The temperatures used during cold sintering are largely dependent on the evaporation point of the solvent. Grain growth has also been observed in some materials cold sintered significantly above the solvent evaporation temperature but below conventional sintering temperatures, this could be used to achieve specific grain sizes and structures.

### 2.3.2 Residual Secondary Phases

In some cases, secondary phases can form during cold sintering, due to reactions between the solid phase and transient solvent or residual solvent after sintering completion. Kang *et al*. used a number of acids in the cold sintering of ZnO to observe their effectiveness as solvent phases. For a $ZnCl_2$ solution, significant amounts of zinc oxychloride phases were observed, with similar results produced when sulfate and nitrate based solvents were used. While the use of such strong solvents is an extreme example, it demonstrates the importance of correct solvent choice for the sintering process to prevent secondary phase formation. Even for more successful solvent phases used to densify ZnO, such as acetic acid and Zn-Ac, small amounts of residual acetate phases have been detected and affect properties.

When $BaTiO_3$ interacts with distilled water, Ba is leached from the material leading to an amorphous Ti-rich surface layer. This preferential leaching is overcome using a solution containing high concentrations of Ba and Ti ions but amorphous material forms which requires a further post CSP crystallisation step at high temperatures.

### 2.3.3 Nanoparticle Manufacture

While the amount of energy required to densify material *via* cold sintering has shown to be significantly reduced, the energy of nanopowder production has not been routinely considered when evaluating the total energy consumed. To produce nanopowders significant amounts of energy or complex chemical reactions are often required, transferring the energy consumption and environmental costs to a different stage of the manufacturing process.

## 3. Applications of Cold Sintering in Radiofrequency Technology

### 3.1 Microwave Dielectric Composites

Microwave (MW) dielectric materials show strong interactions with electromagnetic waves, making them extremely important in modern communications as resonators, filters and substrates (22, 35). The three selective parameters of MW dielectric ceramics are high quality factor (*Qf*), near-zero temperature coefficient of resonant frequency (TCF) and high $\varepsilon_r$ (19, 22, 35).

With fifth generation (5G) network technologies beginning to be utilised and installed in numerous countries, the material challenge is to develop systems of very high resonant frequency and low latency. Whilst fourth generation (4G) systems operate in the 2–8 GHz range, the operating range of 5G systems will eventually be up to 30 GHz. For these 5G systems, the dielectric loss of polymeric substrates used in 4G is too high and other substrates must be investigated (36–39).

Cold sintering has shown promise within this area at The University of Sheffield with the densification of several known MW ceramics achieved at low temperatures. However, none of the early materials such as LMO and NMO exhibited near zero TCF. Consequently, Wang *et al.* (17, 19) has developed

several, two component temperature stable MW ceramic composites *via* CSP.

$Na_{0.5}Bi_{0.5}MoO_4$-$Li_2MoO_4$ (NBMO-LMO) composite samples were produced by mixing NBMO and LMO powders with 5–10 wt% of deionised water and pressing pellets 30 min at 150°C and 200 MPa. Sintered pellets were dried for 24 h at 120°C to remove any residual moisture (22). The NBMO-LMO ceramic composites in this study showed no chemical reaction between the phases during cold sintering and near zero TCF was achieved at ~20% LMO with $\varepsilon_r$ = 17 and *Qf* = 8000 GHz (22) (**Figure 5**).

$(Bi_{0.95}Li_{0.05})(V_{0.9}Mo_{0.1})O_4$-$Na_2Mo_2O_7$(BLVMO-NMO) composites were also sintered by combining the mixtures with 5–10 wt% of deionised water and hot pressing for 30 min at 150°C and 200 MPa. A post sintering drying step of 120°C for 24 h was performed to remove residual moisture (19). Electrical and MW analysis of the BLVMO-NMO showed similar trends to the NBMO-LMO and near zero TCF was obtained at ~20% NMO with $\varepsilon_r$ ~40 and *Qf* = 4000, **Figure 6**.

Although the *Qf* values of these composites do not compete with conventionally sintered ceramics for resonator applications, their properties, ease of integration and low energy consumption show promise for a wide range of novel devices.

## 3.2 Graded-Index Lenses

Graded-index (GRIN) lenses (19, 43) are able to convert a point electromagnetic source to a planar wave and *vice versa*. They are normally used in optics but CSP can be used to fabricate devices from ceramics in MW applications. A MW GRIN lens (19, 22) consists of concentric rings of material, with decreasing $\varepsilon_r$ towards the outer edge of the structure, preferably reaching values close to $\varepsilon_r$ = 1. Dimensions and $\varepsilon_r$ of the layers are tailored to ensure they have the same focal point (O) to convert the incident spherical wave to a plane wave; a schematic GRIN lens design is shown in **Figure 7** and a simulation (CST Microwave Studio, Dassault Systèmes, France) of a working GRIN lens is shown in **Figure 8**.

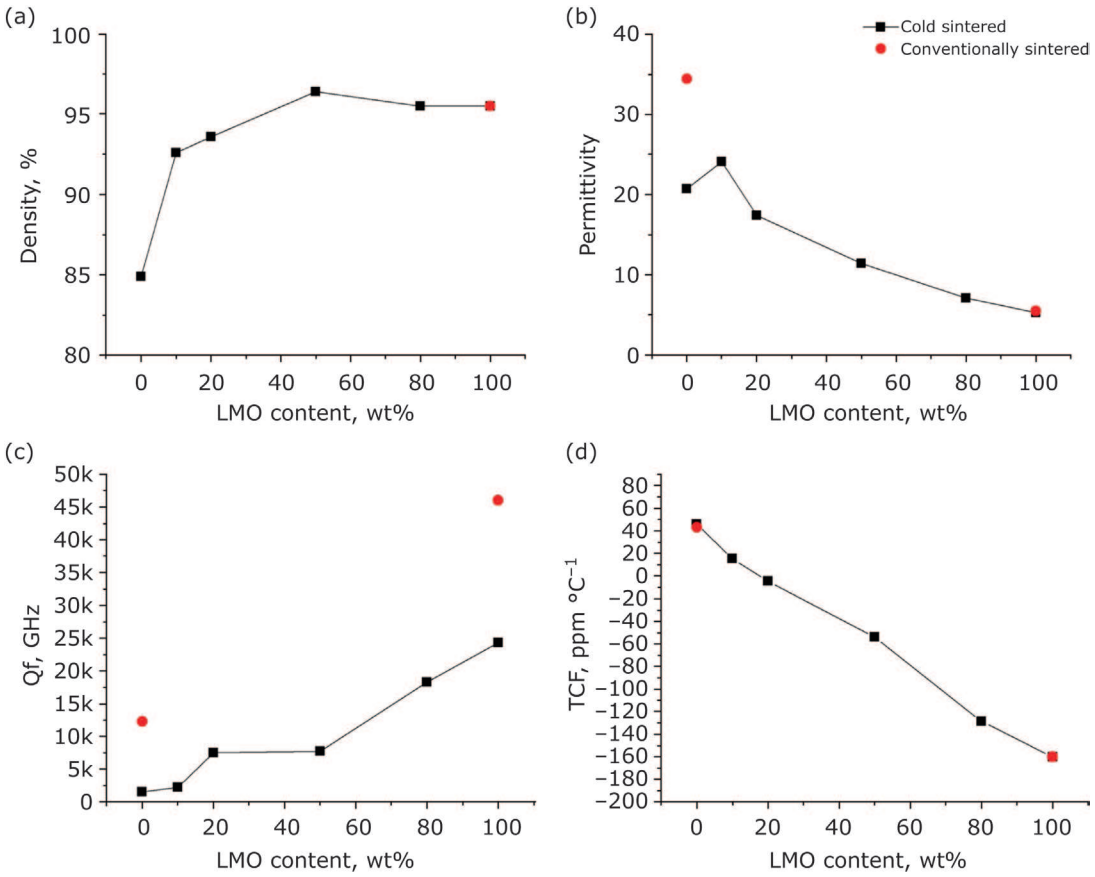


Fig. 5. (a) Density; (b) permittivity; (c) *Qf*; and (d) TCF of NBMO-*x*LMO composite ceramics produced by cold sintering, comparing permittivity to conventional samples produced and measured by Zhou *et al*. (19). Adapted from (19) under Creative Commons Attribution 4.0 International (CC BY 4.0)

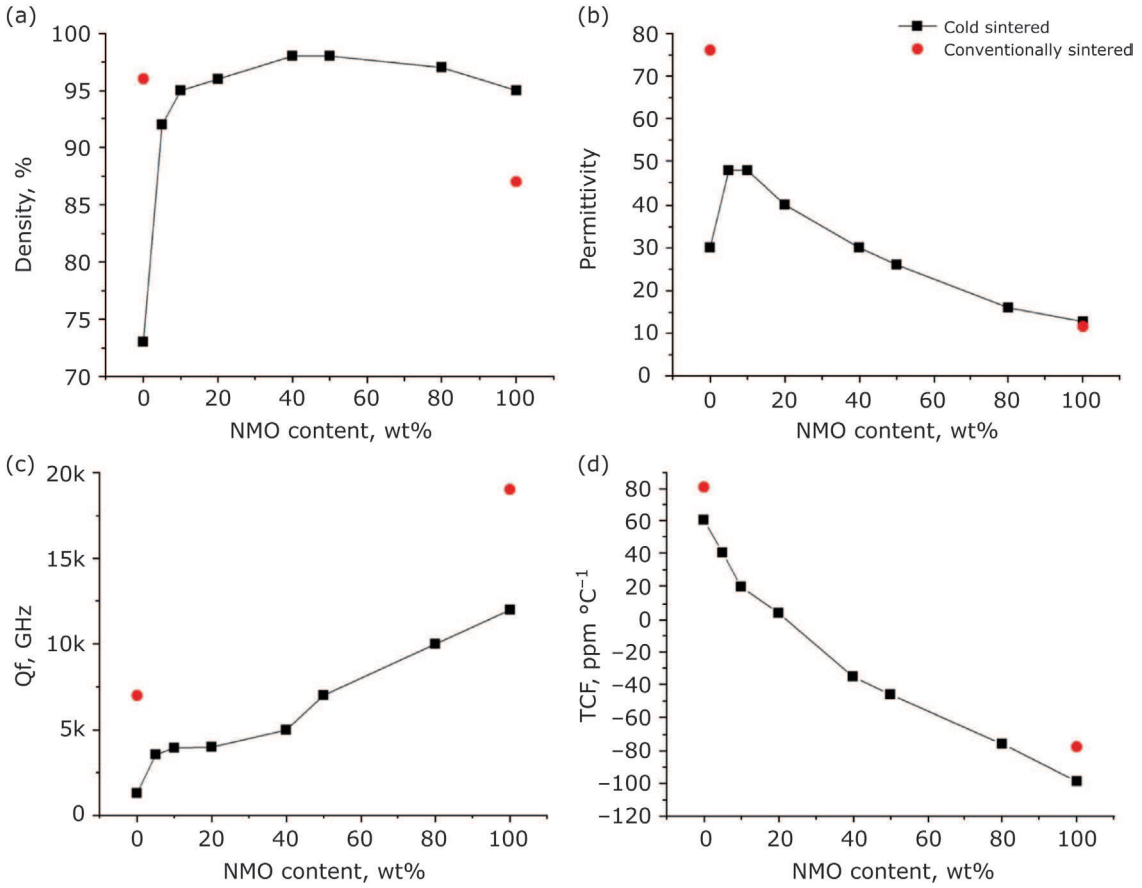


Fig. 6. (a) Density; (b) permittivity; (c) *Qf*; and (d) TCF of cold sintered BLVMO-NMO composite ceramics and conventionally sintered BLVMO and NMO. Adapted from (19) under Creative Commons Attribution 4.0 International (CC BY 4.0)

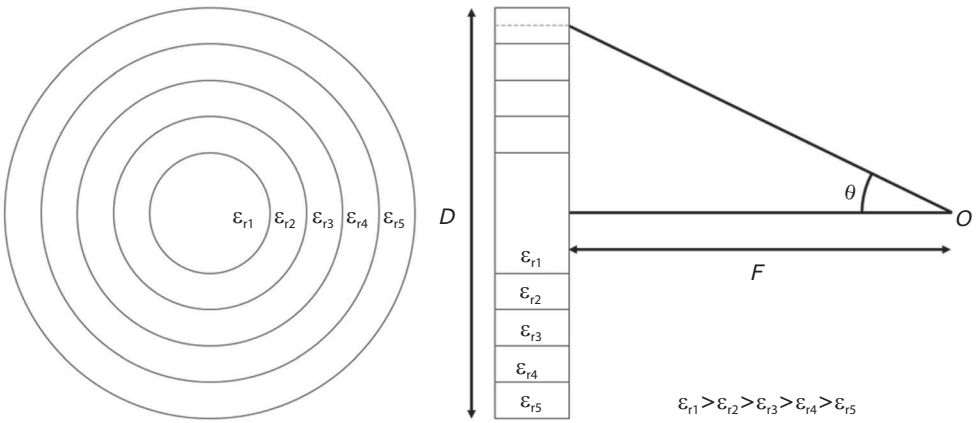


Fig. 7. Schematic of a GRIN lens design principal. Where D is the external diameter of the layer, θ is the angle from focal point (O) to middle of ring and F is the focal length. Reproduced with permission from (22). Further permissions related to this material should be directed to the American Chemical Society (ACS)

The simulated lens was illuminated with an open-ended $K_a$-band waveguide (7.112 mm × 3.556 mm). Across the whole frequency range the boresight directivity was increased from 26 GHz to 40 GHz, the relative increase compared to the case with no lens was between 4.6 dB and 8.5 dB. The simulated BLVMO-NMO and NBMO-LMO lenses exhibited an aperture efficiency ~70% at 26 GHz and ~78% at 34 GHz respectively (19, 22).

 

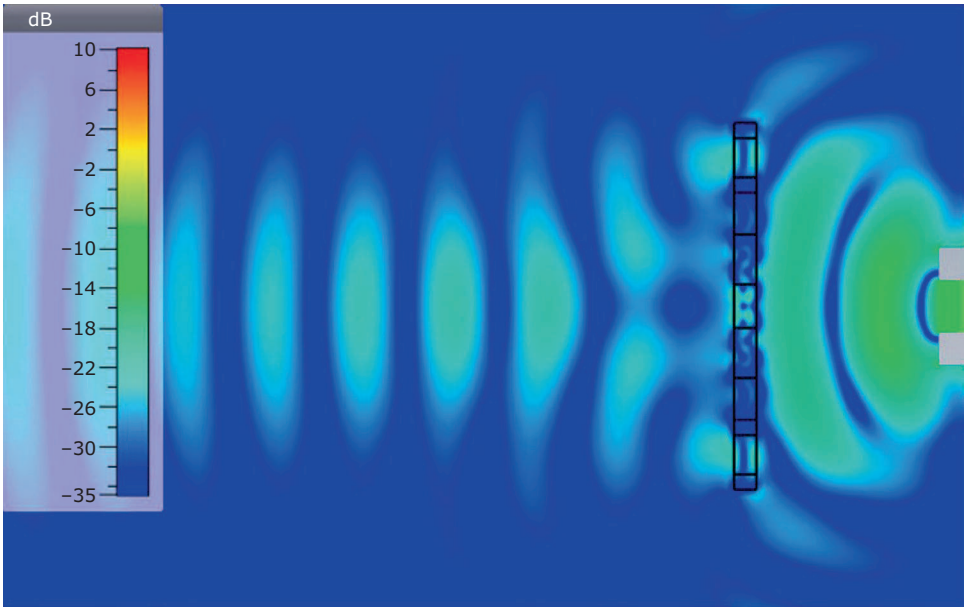


Fig. 8. Simulation of electric fields as a GRIN lens transforms spherical wave fronts into planar waves. Reproduced from (19) under Creative Commons Attribution 4.0 International (CC BY 4.0)

Due to the ability to control lateral dimensions during cold sintering, it is possible to co-sinter multiple layers of ceramics without the detrimental effects of differential shrinkage and divergent thermal expansion coefficients. Wang *et al*. co-sintered three layers of ceramic in the LMO-NBMO system (LMO, NMBO-10 wt% LMO and NMBO-50 wt% LMO) to create a macroscopic ceramic-ceramic composite (22). This demonstrated the ability to utilise cold sintering to produce graded dielectrics and thus illustrated proof of concept for the fabrication of a MW GRIN lens. Simulations were performed to understand the potential efficiency of lenses composed of six concentric rings of radially reducing $\varepsilon_r$, illuminated with a $K_a$-band waveguide between 26–40 GHz. Peak aperture efficiencies were 78% at 34 GHz for the NBMO-LMO lens and 70% at 26 GHz for the BLVMO-NMO lens. Demonstrating high conversion rates between input and output of the lens.

## 3.3 Microstrip Patch Antennas

Microstrip patch antennae (MPA) are a low-profile form of antenna that can be integrated effectively where space and weight restrictions apply and maybe printed onto polymer-based printed circuit boards (PCBs) for mobile device applications (44, 45).

At The University of Sheffield, Wang *et al*. made use of cold sintering to produce an MPA from a calcium titanite-potassium molybdate (CTO-KMO) composite. Composites were produced at 150°C under a uniaxial pressure of 200 MPa for 30 min, achieving high density for all compositions. From energy-dispersive X-ray spectroscopy (EDS) mapping, the authors showed that two chemically discrete regions are present in the composites after cold sintering indicating that no reaction occurs between the two phases during sintering (45).

For 5G antenna substrates, materials should have low $\varepsilon_r$ (<15), a near-zero TCF and high-quality factor (45, 46). In previous studies, the dielectric properties of composites approximately follow known mixing laws and can therefore be tailored to suit specific applications. A CTO-KMO composite produced with 92 wt% KMO had TCF ~–4 ppm °C$^{-1}$, $\varepsilon_r$ = 8.5 and $Qf$ ~11,000 GHz. This composition was then used to create a cold sintered MPA which operates at 2.51 GHz with a 62% radiation efficiency (**Figure 9**). The combination of high antenna performance and low temperature densification demonstrate the potential for the direct fabrication of antenna substrates onto PCBs (45).

## 3.4 Multilayer Ceramic Capacitors

Multilayer ceramic capacitors (MLCCs) consist of alternate layers of ceramic and metallic electrode and over three trillion are produced every year (20). MLCCs are conventionally sintered at high temperatures which presents several challenges, not least the electrode melting point and chemical compatibility with the ceramic.

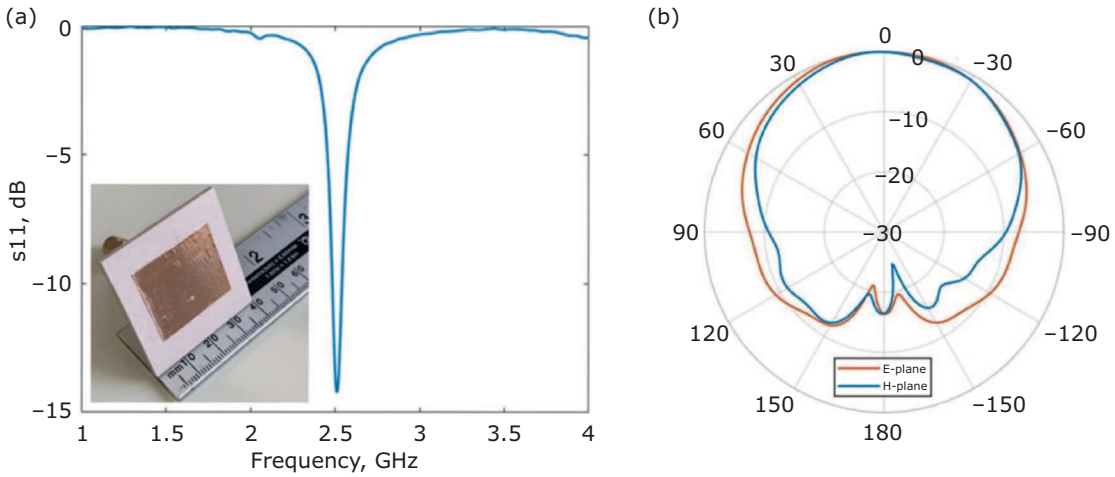


Fig. 9. (a) Efficiency; and (b) radiation pattern of a microstrip patch antenna (inset (a)) fabricated from CTO-KMO

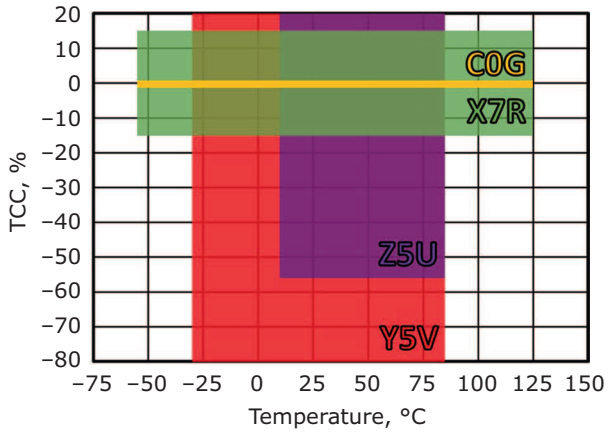


Fig. 10. Comparison of commonly used capacitor categories, according to TCC and temperature

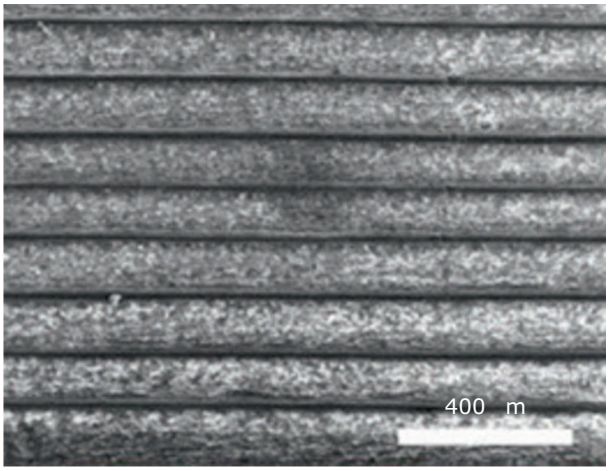


Fig. 11. Cold sintered multilayer capacitor with C0G characteristics fabricated at 150°C from BLVMO-0.2NMO. Reproduced with permission from (20)

Capacitors are used in a wide variety of applications and conditions and they are characterised by the temperature dependency of their properties. C0G (or NP0) Class 1 dielectric materials do not show a significant variation in capacitance over a wide range of temperatures. Materials with positive and negative temperature coefficients of capacitance (TCC) can be mixed to create a temperature stable ceramic composite. **Figure 10** compares the TCC of several common Class 2 and C0G capacitors.

The TCC of BLVMO and NMO ceramics are approximately +81 ppm $°C^{-1}$ and −99 ppm $°C^{-1}$ respectively. The combination of these materials creates temperature stable composites <10 ppm $°C^{-1}$ with low dielectric loss (tan $\delta \approx 0.001$) and $\varepsilon_r = 40$ (19, 20). Using BLVMO-*x*NMO ($x = 0.2$) composites, researchers at The University of Sheffield have demonstrated the use of cold sintering to produce multilayer ceramic capacitors with comparable properties to conventional calcium zirconate C0G MLCCs manufactured at 1100°C (20). Laminated stacks were made from tape cast BLVMO-NMO with screen printed silver electrodes. After binder burnout, at 180°C for 3 h, stacks were exposed to water vapour in a sealed beaker at 80°C. The moistened stacks were then cold sintered at 150°C under 100 MPa of pressure for 30 min. The SEM image of the cross-section of the cold sintered MLCC in **Figure 11** shows the dielectric layers are well densified, well laminated

and unwarped. The Ag electrodes also appear well defined indicating no reaction at the metal-ceramic interface (20). The room temperature $\varepsilon_r$ and loss at 1 MHz were found to be 39 and 0.01 respectively and the TCC was within 0.013% up to 150°C.

## 4. Commercialisation: Challenges for Scale-up and Complex Structures

Some ceramic materials require high pressures to achieve the desired densification. To scale up the CSP to produce larger components therefore, a significant increase in applied pressure will be required compared to laboratory scale. Cold sintering is currently a batch process with a small number of samples produced. For this technology to be adopted more widely, rates of manufacture should be increased. Currently only simple two-dimensional and pellet shapes have been reported. Many potential applications for cold sintering ceramics will require more complex shapes, which could be achieved by creating near net-shape die pieces, although this brings its own challenges of die filling and variations in pressure across the component during sintering.

## 5. Conclusion

Alongside the reduction in manufacturing energy consumption, lower sintering temperatures allow densification of materials that would otherwise react, decompose or volatilise. This new area of research is gaining traction as more materials and prototype components are developed. Cold sintering has the potential to be a game changing technology in ceramic processing and component manufacturing and work at The University of Sheffield has demonstrated several potential avenues for cold sintering to create devices and composites which are not achievable through conventional sintering.

## Acknowledgements

The authors would like to acknowledge the support of the Johnson Matthey Strategic Fund and the Engineering and Physical Science Research Council (EPSRC) grants, EP/L017563/1 and EP/N010493/1.

## References

1. R. M. German, *Powder Metall.*, 2013, **56**, (2), 117
2. D. S. B. Heidary, M. Lanagan and C. A. Randall, *J. Eur. Ceram. Soc.*, 2018, **38**, (4), 1018
3. T. Kimura, Q. Dong, S. Yin, T. Hashimoto, A. Sasaki and T. Sato, *J. Eur. Ceram. Soc.*, 2013, **33**, (5), 1009
4. C. A. Randall, S. F. Wang, D. Laubscher, J. P. Dougherty and W. Huebner, *J. Mater. Res.*, 1993, **8**, (4), 871
5. H.-I. Hsiang, C.-S. Hsi, C.-C. Huang and S.-L. Fu, *J. Alloys Compd.*, 2008, **459**, (1–2), 307
6. "Sintering of Advanced Ceramics", eds. C. A. Handwerker, J. E. Blendell and W. Kaisser, Ceramic Transactions, Vol. 7, American Ceramic Society, Ohio, USA, 1990, 789 pp
7. M. Biesuz and V. M. Sglavo, *J. Eur. Ceram. Soc.*, 2019, **39**, (2–3), 115
8. J. A. Downs and V. M. Sglavo, *J. Am. Ceram. Soc.*, 2013, **96**, (5), 1342
9. M. Al. Minnath, 'Metals and Alloys for Biomedical Applications', in "Fundamental Biomaterials: Metals", eds. P. Balakrishnan, M. S. Sreekala and S. Thomas, Ch. 7, Elsevier Ltd, Duxford, UK, 2018, pp. 167–174
10. T. Herisson de Beauvoir, A. Sangregorio, I. Cornu, C. Elissalde and M. Josse, *J. Mater. Chem. C*, 2018, **6**, (9), 2229
11. C. Elissalde, U.-C. Chung, M. Josse, G. Goglio, M. R. Suchomel, J. Majimel, A. Weibel, F. Soubie, A. Flaureau, A. Fregeac and C. Estournès, *Scripta Mater.*, 2019, **168**, 134
12. H. Kähäri, M. Teirikangas, J. Juuti and H. Jantunen, *J. Am. Ceram. Soc.*, 2014, **97**, (11), 3378
13. J. Guo, H. Guo, A. L. Baker, M. T. Lanagan, E. R. Kupp, G. L. Messing and C. A. Randall, *Angew. Chemie*, 2016, **128**, (38), 11629
14. N. Yamasaki, K. Yanagisawa, M. Nishioka and S. Kanahara, *J. Mater. Sci. Lett.*, 1986, **5**, (3), 355
15. K. Yanagisawa, K. Ioku and N. Yamasaki, *J. Am. Ceram. Soc.*, 2005, **80**, (5), 1303
16. K. Hosoi, T. Hashida, H. Takahashi, N. Yamasaki and T. Korenaga, *J. Am. Ceram. Soc.*, 1996, **79**, (10), 2771
17. J.-P. Maria, X. Kang, R. D. Floyd, E. C. Dickey, H. Guo, J. Guo, A. Baker, S. Funihashi and C. A. Randall, *J. Mater. Res.*, 2017, **32**, (17), 3205
18. H. Kähäri, M. Teirikangas, J. Juuti and H. Jantunen, *J. Am. Ceram. Soc.*, 2015, **98**, (3), 687
19. D. Wang, S. Zhang, D. Zhou, K. Song, A. Feteira, Y. Vardaxoglou, W. Whittow, D. Cadman and I. M. Reaney, *Materials*, 2019, **12**, (9), 1370
20. D. Wang, D. Zhou, K. Song, A. Feteira, C. A. Randall and I. M. Reaney, *Adv. Electron. Mater.*, 2019, **5**, (7), 1900025
21. S. S. Faouri, A. Mostaed, J. S. Dean, D. Wang, D. C. Sinclair, S. Zhang, W. G. Whittow,

 

Y. Vardaxoglou and I. M. Reaney, *Acta Mater.*, 2019, **166**, 202

22. D. Wang, D. Zhou, S. Zhang, Y. Vardaxoglou, W. G. Whittow, D. Cadman and I. M. Reaney, *ACS Sustain. Chem. Eng.*, 2018, **6**, (2), 2438
23. T. K. Gupta, *J. Am. Ceram. Soc.*, 1990, **73**, (7), 1817
24. T. K. Roy, D. Bhowmick, D. Sanyal and A. Chakrabarti, *Ceram. Int.*, 2008, **34**, (1), 81
25. X. Kang, R. Floyd, S. Lowum, M. Cabral, E. Dickey and J.P. Maria, *J. Am. Ceram. Soc.*, 2019, **102**, (8), 4459
26. S. Funahashi, J. Guo, H. Guo, K. Wang, A. L. Baker, K. Shiratsuyu and C. A. Randall, *J. Am. Ceram. Soc.*, 2016, **100**, (2), 546
27. J. Gonzalez-Julian, K. Neuhaus, M. Bernemann, J. Pereira da Silva, A. Laptev, M. Bram and O. Guillon, *Acta Mater.*, 2018, **144**, 116
28. J. Nie, Y. Zhang, J. M. Chan, R. Huang and J. Luo, *Scripta Mater.*, 2018, **142**, 79
29. R. Boston, J. Guo, S. Funahashi, A. L. Baker, I. M. Reaney and C. A. Randall, *RSC Adv.*, 2018, **8**, (36), 20372
30. H. Guo, J. Guo, A. Baker and C. A. Randall, *J. Am. Ceram. Soc.*, 2016, **100**, (2), 491
31. C. Vakifahmetoglu, J. F. Anger, V. Atakan, S. Quinn, S. Gupta, Q. Li, L. Tang and R. E. Riman, *J. Am. Ceram. Soc.*, 2016, **99**, (12), 3893
32. J.-P. Ma, X.-M. Chen, W.-Q. Ouyang, J. Wang, H. Li and J.-L. Fang, *Ceram. Int.*, 2018, **44**, (4), 4436
33. M. C. Blanco-Lopez, B. Rand and F. L. Riley, *J. Eur. Ceram. Soc.*, 1997, **17**, (2–3), 281
34. M. Bäurer, H. Kungl and M. J. Hoffmann, *J. Am. Ceram. Soc.*, 2009, **92**, (3), 601
35. N. M. Alford, S. J. Penn, A. Templeton, X. Wang, J. C. Gallop, N. Klein, C. Zuccaro and P. Filhol, 'Microwave Dielectrics', IEE Colloquium on Electro-Technical Ceramics – Processing, Properties and Applications, The Institution of Engineering and Technology, London, UK, 14th November, 1997
36. I. F. Akyildiz, S. Nie, S.-C. Lin and M. Chandrasekaran, *Comput. Networks*, 2016, **106**, 17
37. E. Hossain and M. Hasan, *IEEE Instrum. Meas. Mag.*, 2015, **18**, (3), 11
38. G. Ancans, V. Bobrovs, A. Ancans and D. Kalibatiene, *Procedia Comput. Sci.*, 2017, **104**, 509
39. P. Wang, Y. Li, L. Song and B. Vucetic, *IEEE Commun. Mag.*, 2015, **53**, (1), 168
40. D. Zhou, C. A. Randall, L.-X. Pang, H. Wang, J. Guo, G.-Q. Zhang, Y. Wu, K.-T. Guo, L. Shui and X. Yao, *Mater. Chem. Phys.*, 2011, **129**, (3), 688
41. J. Guo, S. S. Berbano, H. Guo, A. L. Baker, M. T. Lanagan and C. A. Randall, *Adv. Funct. Mater.*, 2016, **26**, (39), 7115
42. D. Zhou, C. A. Randall, H. Wang, L.-X. Pang and X. Yao, *J. Am. Ceram. Soc.*, 2010, **93**, (4), 1096
43. S. Zhang, R. K. Arya, S. Pandey, Y. Vardaxoglou, W. Whittow and R. Mittra, *IET Microwaves Antennas Propag.*, 2016, **10**, (13), 1411
44. L. V. Blake and M. W. Long, "Antennas: Fundamentals, Design, Measurement", 3rd Edn., SciTech Publishing, Raleigh, USA, 2009, 503 pp
45. D. Wang, S. Zhang, G. Wang, Y. Vardaxoglou, W. Whittow, D. Cadman, D. Zhou, K. Song and I. M. Reaney, *Appl. Mater. Today*, 2020, **18**, 100519
46. I. M. Reaney and D. Iddles, *J. Am. Ceram. Soc.*, 2006, **89**, (7), 2063

## The Authors

Jessica Andrews completed an MEng in Materials Science and Engineering in 2016. She is now a PhD student within the Functional Materials and Devices Group at The University of Sheffield. Supervised by Professor Reaney and sponsored by Johnson Matthey, her project is focused on developing methods of cold sintering for several ceramic materials and polymer-ceramic composites.

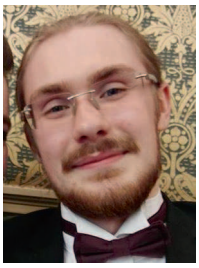

Daniel Button originally graduated at The University of Sheffield with an MEng in Materials Science and Engineering in 2017 and is currently a PhD student in the Functional Materials and Devices at the same university. He is working on a project sponsored by Johnson Matthey, investigating the cold sintering of ZnO and its possible use cases for industrial application.

 

Ian M. Reaney was appointed Professor in Ceramics in 2007 and in 2017 to the Dyson Chair in Ceramics at The University of Sheffield. Ian's research interests are in development of MW and piezoelectric materials and functional glasses. He's published more than 400 papers and given over 100 invited, keynote and plenary talks at international conferences. His h-index is 63 and his papers have received >16,000 citations. He won the Edward C. Henry award in 2002, best knowledge transfer partnership building on EPSRC funded research in 2009 and the Verulam Medal in 2017. He is European site director of the Centre for Dielectrics and Piezoelectrics.